

AJNR

This information is current as
of January 12, 2025.

***IDH* Status in Brain Gliomas Can Be Predicted by the Spherical Mean MRI Technique**





Vojtech Sedlák, Milan Nemý, Martin Májovský, Adéla
Bubeníková, Love Engstrom Nordin, Tomáš Moravec, Jana
Engelová, Dalibor Sila, Dora Konečná, Tomáš Belsan, Eric
Westman and David Netuka

AJNR Am J Neuroradiol 2025, 46 (1) 121-128

doi: <https://doi.org/10.3174/ajnr.A8432>

<http://www.ajnr.org/content/46/1/121>

IDH Status in Brain Gliomas Can Be Predicted by the Spherical Mean MRI Technique

Vojtěch Sedlák,  Milan Němý,  Martin Májovský, Adéla Bubeníková,  Love Engstrom Nordin, Tomáš Moravec, Jana Engelová, Dalibor Sila, Dora Konečná, Tomáš Belšan,  Eric Westman, and David Netuka



ABSTRACT

BACKGROUND AND PURPOSE: Diffuse gliomas, a heterogeneous group of primary brain tumors, have traditionally been stratified by histology, but recent insights into their molecular features, especially the *IDH* mutation status, have fundamentally changed their classification and prognosis. Current diagnostic methods, still predominantly relying on invasive biopsy, necessitate the exploration of noninvasive imaging alternatives for glioma characterization.

MATERIALS AND METHODS: In this prospective study, we investigated the utility of the spherical mean technique (SMT) in predicting the *IDH* status and histologic grade of adult-type diffuse gliomas. Patients with histologically confirmed adult-type diffuse glioma underwent a multiparametric MRI examination using a 3T system, which included a multishell diffusion sequence. Advanced diffusion parameters were obtained using SMT, diffusional kurtosis imaging, and ADC modeling. The diagnostic performance of studied parameters was evaluated by plotting receiver operating characteristic curves with associated area under curve, specificity, and sensitivity values.

RESULTS: A total of 80 patients with a mean age of 48 (SD, 16) years were included in the study. SMT metrics, particularly microscopic fractional anisotropy (μ FA), intraneurite voxel fraction, and μ FA to the third power (μ FA³), demonstrated strong diagnostic performance (all AUC = 0.905, 95% CI, 0.835–0.976; $P < .001$) in determining *IDH* status and compared favorably with diffusional kurtosis imaging and ADC models. These parameters also showed a strong predictive capability for tumor grade, with intraneurite voxel fraction and μ FA achieving the highest diagnostic accuracy (AUC = 0.937, 95% CI, 0.880–0.993; $P < .001$). Control analyses on normal-appearing brain tissue confirmed the specificity of these metrics for tumor tissue.

CONCLUSIONS: Our study highlights the potential of SMT for noninvasive characterization of adult-type diffuse gliomas, with a potential to predict *IDH* status and tumor grade more accurately than traditional ADC metrics. SMT offers a promising addition to the current diagnostic toolkit, enabling more precise preoperative assessments and contributing to personalized treatment planning.

ABBREVIATIONS: AK = axial kurtosis; AUC = area under the curve; CEST = chemical exchange saturation transfer; DKI = diffusional kurtosis imaging; INVF = intraneurite voxel fraction; μ FA = microscopic fractional anisotropy; MK = mean kurtosis; MKT = mean kurtosis tensor; RK = radial kurtosis; ROC = receiver operating characteristic; SMT = spherical mean technique; TMD = transverse microscopic diffusivity; WHO = World Health Organization

Diffuse gliomas, a significant portion of primary brain tumors, present challenges in diagnosis and treatment. These tumors have traditionally been classified into low-grade and high-grade gliomas based on histologic features, with the former generally

associated with a better prognosis.¹ The introduction of molecular markers, notably the isocitrate dehydrogenase (*IDH*) mutation, has revolutionized this classification, leading to a more nuanced understanding that combines histologic and molecular

Received May 14, 2024; accepted after revision July 10.


From the Department of Radiology (V.S., T.B.), Military University Hospital, Prague, Czech Republic; Division of Clinical Geriatrics (M.N., L.E.N., E.W.), Department of Neurobiology, Care Sciences and Society, Center for Alzheimer Research, Karolinska Institute, Stockholm, Sweden; Department of Biomedical Engineering and Assistive Technology (M.N.), Czech Institute of Informatics, Robotics and Cybernetics, Czech Technical University in Prague, Prague, Czech Republic; Department of Neurosurgery and Neurooncology (M.M., A.B., T.M., D.K., D.N.), First Faculty of Medicine, Charles University and Military University Hospital, Prague, Czech Republic; Department of Diagnostic Medical Physics (L.E.N.), Karolinska University Hospital Solna, Stockholm, Sweden; Radiodiagnostic Department (J.E.), Proton Therapy Center Czech Ltd, Prague, Czech Republic; Department of Neurosurgery and Spine Surgery (D.S.), Arberlandklinik Viechtach, Germany; and Department of Neuroimaging (E.W.), Centre for Neuroimaging Science, Institute of Psychiatry, Psychology, and Neuroscience, King's College London, London, UK.

This research was supported by Charles University, project GA UK No. 222623. Institutional support MO1012 was by the Ministry of Defense of the Czech

Republic, and Cooperation Neuroscience was by Charles University. Research by M.N. was partially supported by the institutional resources of Czech Technical University in Prague and Karolinska Institute.

The funders of the study had no role in the study design or the collection, analysis, and interpretation of data, writing of the report, or decision to submit the manuscript for publication.

Please address correspondence to Martin Májovský, MD, PhD, Department of Neurosurgery and Neurooncology, First Faculty of Medicine, Charles University, U Vojenské nemocnice 1200, Prague, 16000 Czech Republic; e-mail: martin.majovsky@uvn.cz

 Indicates open access to non-subscribers at www.ajnr.org

 Indicates article with online supplemental data.

<http://dx.doi.org/10.3174/ajnr.A8432>

characteristics for prognosis and treatment-planning. The 2016 World Health Organization (WHO) Classification of the Tumors of the Central Nervous System,² further refined in 2021, highlights the critical role of *IDH* mutation status in determining therapeutic approaches and predicting patient outcomes.

Conventional MRI techniques are instrumental in initial glioma assessment. However, their specificity and sensitivity in distinguishing *IDH*-mutant and *IDH*-wild-type gliomas are limited, often requiring invasive biopsy for accurate molecular diagnosis.³

Recent advances in diffusion MRI techniques have shown some promise in better characterizing and stratifying gliomas. These techniques have the ability to evaluate tissue microstructure and quantitatively assess the non-Gaussian diffusion behavior of water molecules in tissues.^{4,5} Among these, the ADC model and diffusional kurtosis imaging (DKI) have been extensively studied,⁶⁻¹⁰ providing insights into tumor grade and cellular density.

A common pitfall of the above-mentioned models is their inability to disentangle the effects of axonal architecture from the diffusion parameters of the underlying brain tissue.¹¹ This pitfall is a substantial drawback, because neurite microarchitecture varies widely not only between individuals¹² but also in different brain regions of a single patient and changes across time.¹³ The inability to separate these intra- and extra-axonal compartments makes it difficult for traditional diffusion techniques to trace the origin of the pathologic changes in the diffusion patterns. This issue is especially important in the case of diffuse gliomas, in which due to their infiltrative growth, the axonal circuitry remains relatively well-preserved and can obscure potentially important changes due to the presence of underlying pathology.

The spherical mean technique (SMT) emerges as a promising solution to these challenges.^{14,15} SMT is a recently proposed multicompartmental model that is capable of reconstructing diffusion-based parameters unconfounded by axonal microstructure and capable of separating the diffusion parameters within the intra-axonal and extra-axonal compartments. The output parameters of this method are, therefore, not burdened by intra- and intersubject variability in axonal architecture and are potentially more specific to diffusional alteration happening within the pathologic tissue itself. For example, the fractional anisotropy of the classic diffusion tensor model encodes both the microscopic diffusion process and the fiber-orientation distribution. In contrast, the microscopic fractional anisotropy of SMT is sensitive solely to microscopic diffusion and factors out the intravoxel fiber-orientation distribution. This approach could lead to more specific and clinically relevant markers for noninvasive glioma assessment.¹⁵ To date, SMT has been demonstrated to improve lesion detection in the spinal cord of patients with MS;¹⁶ however, this is the first study investigating its potential in neuro-oncology.

The hypothesis of this study is that SMT could outperform traditional diffusion MRI metrics in predicting the *IDH* status and histologic grade of adult-type diffuse gliomas due to its ability to separate diffusion characteristics of intra- and extra-axonal water diffusion. Our aim was to validate the clinical applicability of SMT, potentially enhancing the accuracy of preoperative glioma characterization and supporting more personalized treatment decisions.

MATERIALS AND METHODS

This single-center prospective study was approved by the institutional review board at Military University Hospital, Prague, Czech Republic, and all patients provided written informed consent.

Patient Selection

Adult patients referred to the Military University Hospital, Prague, Czech Republic, between January 2022 and May 2023, with a working diagnosis of adult-type diffuse glioma of any grade have been randomly selected and included in the study. These patients then underwent preoperative MRI and subsequent tumor sampling with histopathologic and molecular/genetic analyses. Patients were excluded if the histopathologic examination confirmed other diagnosis than supratentorial adult-type diffuse glioma, in cases of technically inadequate MRI examination, or in cases with unavailable or incomplete data from genetic analysis.

Data Acquisition

MRI Acquisition. All patients underwent MRI scans immediately (ie, within 24 hours) before biopsy or resection using a 3T MR system GE Discovery 750W (GE Healthcare). The protocol consisted of 2 groups of pulse sequences: 3D structural sequences (T1WI BRAVO, T2WI FLAIR Cube [GE Healthcare], T2WI Cube, 3D T2 susceptibility-weighted angiography [SWAN], and contrast-enhanced T1WI [BRAVO]); and a multishell diffusion sequence (134 non- B_0 gradient directions, 11 B_0 volumes, and 7 non- B_0 b-values). We used the MRtrix gen-scheme (https://github.com/MRtrix3/mrtrix3/blob/master/bin/gen_scheme) for optimal shell sampling.¹⁷ For more information about the imaging protocol, see the Online Supplemental Data. The whole processing pipeline for the MRI data is outlined in Fig 1.

Histopathologic Data and *IDH* Status. Each patient underwent thorough histologic grading and determination of *IDH* status as part of the standard clinical management protocol. The histologic grade was established using the 5th edition of the World Health Organization Classification of Tumors of the Central Nervous System.² For further analysis, tumors were split into 2 groups, low-grade glioma (WHO grade 2) and high-grade glioma (WHO grades 3 and 4). The *IDH* status was determined using next-generation DNA sequencing. Tissue sampling (via biopsy or resection) was performed within 24 hours after the MRI examination.

Tumor Segmentation

Glioma segmentation was performed using ITK-SNAP (Version 4.0.1; www.itksnap.org), with T1WI, T2WI, FLAIR, and contrast-enhanced T1WI (Fig 1F). An experienced neuroradiologist (V.S.) performed semiautomatic segmentation using the tissue-classification pipeline of ITK-SNAP (Fig 1G). The output segmentation masks included the following: 1) enhancing tumor, 2) nonenhancing tumor, 3) central necrosis, 4) peritumoral T2 hyperintensity (assumed to predominantly represent vasogenic edema if not clearly a part of the nonenhancing tumor), and 5) hemorrhage (to exclude hemorrhagic regions from diffusion and perfusion analysis due to artifacts and possible confounding factors). Tumor enhancement or nonenhancement was verified using motion-corrected subtraction of pre- and postcontrast T1WI. The presence

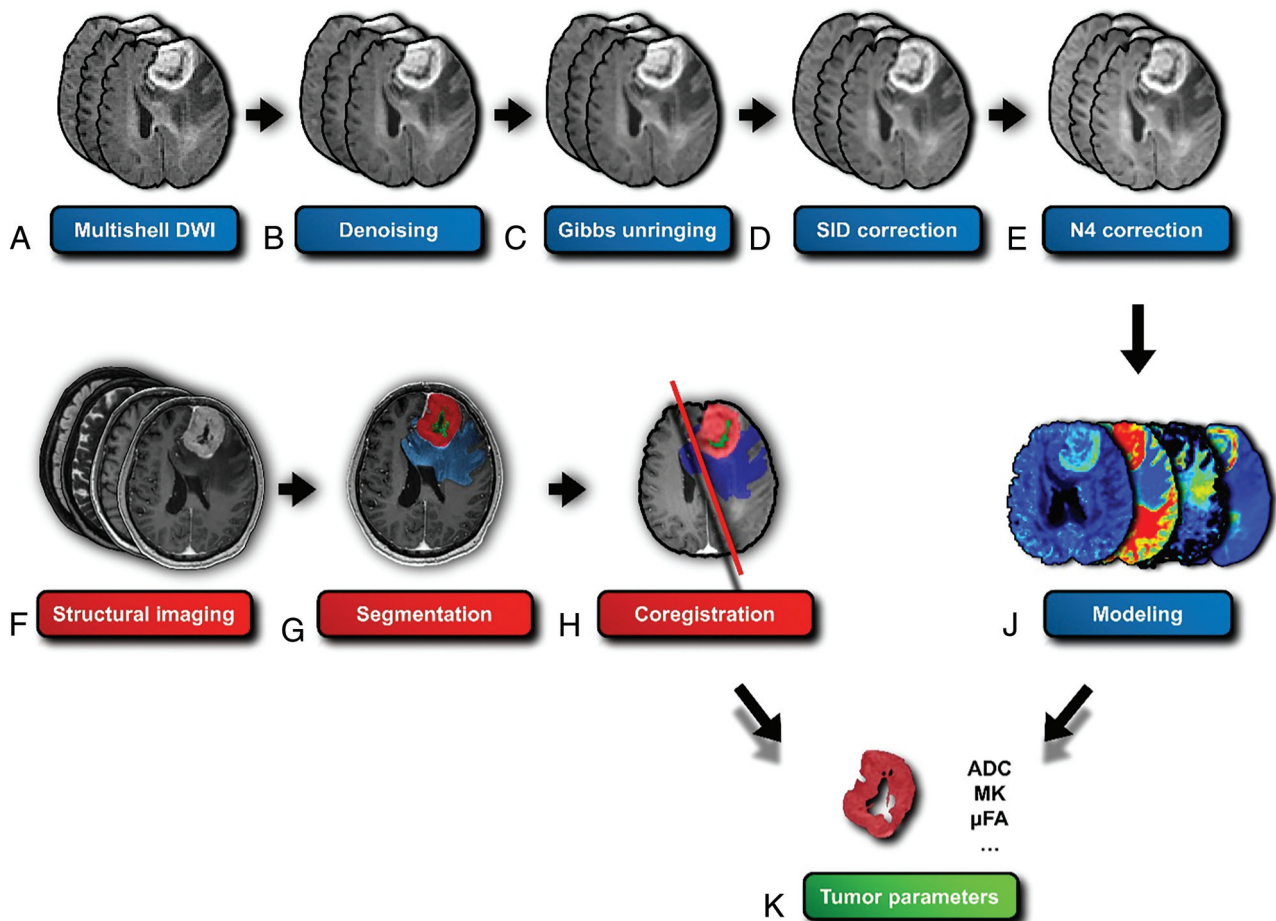


FIG 1. Diffusion data-processing pipeline for glioma assessment. Initial multishell DWI (A) is followed by Marchenko-Pastur principal component analysis (MP-PCA) denoising (B) to reduce noise. Subsequent steps include Gibbs ringing artifact removal (C), susceptibility-induced distortion (SID) correction (D), and N4 bias field correction (E) to improve image quality. Structural imaging (F) is used for tumor segmentation (G), which is then coregistered (H) with the diffusion data. Modeling of the diffusion data (J) enables extraction of tumor parameters (K), such as ADC, MK, and μ FA. The I letter was intentionally omitted to improve readability.

of enhancing tumor, central necrosis, T2 FLAIR mismatch, and hemorrhage was used in the subsequent analysis, with respective binary variables indicating the presence or absence of each feature. Illustration of tumor segmentation and generation of tumoral masks is shown in Fig 2.

Extraction of Neuroimaging Parameters

Diffusion Analysis. Diffusion data (Fig 1A) were preprocessed using FSL (Version 6.0.6; <http://www.fmrib.ox.ac.uk/fsl>), MRtrix3 (Version 3.0.4; <https://www.mrtrix.org/2022/12/16/mrtrix-3-0-4-release/>), and Advanced Normalization Tools (Version 2.5.00, ANTs; <http://stnava.github.io/ANTs/>) toolkits. Preprocessing included the following: 1) Marchenko-Pastur principal component analysis denoising (Fig 1B),¹⁸ 2) Gibbs ringing removal (Fig 1C),¹⁹ 3) motion and eddy current distortion correction,²⁰ 4) susceptibility-induced distortion correction (Fig 1D),²¹ and 5) N4 bias field correction (Fig 1E).²²

DKI, ADC, and DTI modeling (Fig 1J) were performed using the Diffusion Imaging in Python (DIPY) toolbox (Version 1.7.0; <https://dipy.org/>), with ADC and DTI using only $b = 0$ and $b = 1000$ shells. SMT maps were reconstructed using the original code introduced by Kaden et al,^{14,15} available at github.com/

ekaden/smt. Comparison of maps showing ADC, DTI, DKI, and SMT models in a selected tumor sample are shown in the Online Supplemental Data.

Diffusion Parameter Extraction. After coregistering the structural images with their respective tumor segmentation masks to the diffusion space using ITK-SNAP (Fig 1H), we overlaid the tumor masks onto the diffusion maps (enhancing tumor mask in case of enhancing tumors, nonenhancing tumor mask in case of nonenhancing tumors). Then, we extracted the intensity values for each voxel within the tumor area. The acquired data sets for each patient were converted into a NumPy array I (Version 1.25.0; <https://numpy.org/doc/stable/release/1.25.0-notes.html>; Python 3.10), and the mean values for each parameter were extracted using the SciPy library (Version 1.10; <https://docs.scipy.org/doc/scipy-1.10.1/>; Python 3.10). In total, 17 diffusion parameters were extracted from the ADC, DTI, DKI, and SMT models (Fig 1K), all using the same approach.

Statistical Analysis

Prediction of IDH Status and Histologic Grade. The primary objective was to assess the association among IDH status, glioma

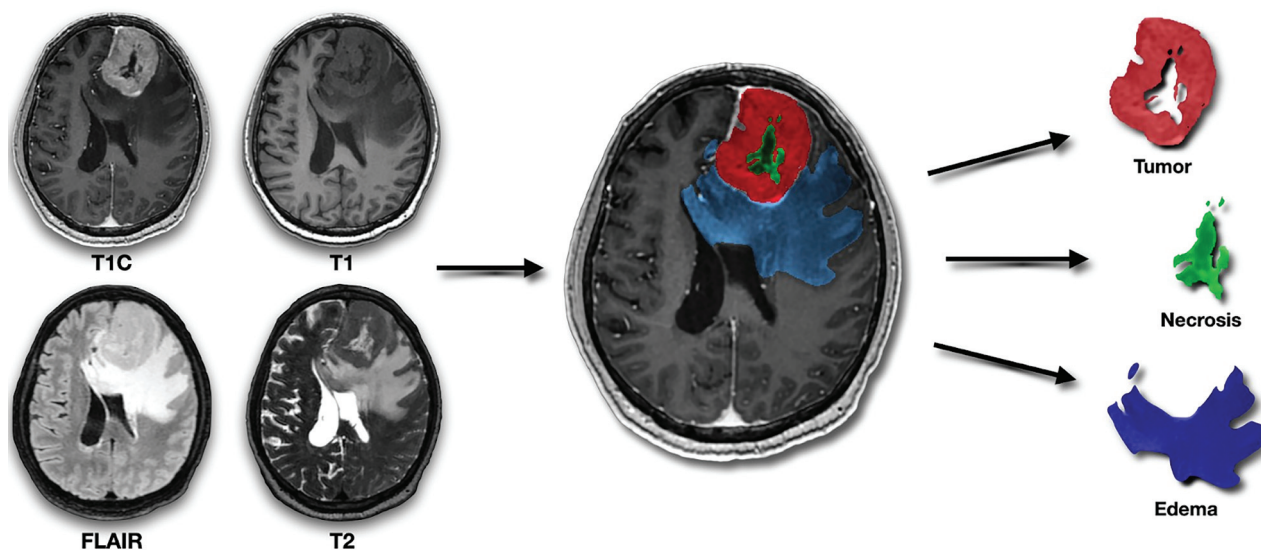


FIG 2. Illustration of tumor segmentation and generation of tumoral masks. The figure demonstrates the segmentation of gliomas using 4 image sequences (from left to right and top to bottom: contrast-enhanced T1-weighted, T1-weighted, FLAIR, and T2-weighted). These masks are subsequently coregistered with diffusion data sets.

Table 1: Patient characteristics^a

Characteristic	Result
No. of patients	80
Age, mean (yr)	48 (SD, 16)
HGG	43 (54)
IDHmt	46 (58)
Male sex	49 (61)
Postcontrast enhancement	46 (58)
Necrosis	31 (39)
T2 FLAIR mismatch	6 (8)
Hemorrhage	24 (30)

Note:—HGG indicates high-grade glioma; IDHmt, *IDH*-mutant.

^aUnless otherwise noted, data represent the number of patients; data in parentheses are percentages.

grade, and the SMT, DKI, and ADC parameters. Receiver operating characteristic (ROC) curves were generated using the *pROC* library (<https://bmcbioinformatics.biomedcentral.com/articles/10.1186/1471-2105-12-77>) to assess the diagnostic performance of the models for predicting *IDH* status and glioma grade. Optimal decision thresholds were identified by area under the curve (AUC) and Youden *J* values for sensitivity and specificity. To quantify the strength and direction of the relationships between the studied diffusion metrics and both *IDH* and glioma grades, we created a correlation matrix by calculating Pearson coefficients using the *gplots* (<https://www.rdocumentation.org/packages/gplots/versions/3.1.3.1>) and *corrplot* (<https://www.rdocumentation.org/packages/corrplot/versions/0.92>) libraries. Statistical analyses were conducted in R statistical and computing software (Version 4.0.3; <http://www.r-project.org/>) with a significance level of .05.

RESULTS

Patient Characteristics

Among 108 patients with a working diagnosis of adult-type diffuse glioma, 28 were excluded for malignancies other than adult-type diffuse glioma. No patients were excluded for technical reasons. Therefore, the final study cohort consisted of 80 patients

with histologically confirmed adult-type diffuse glioma, with a mean age of 48 (SD, 16) years (range, 21–83 years). Most patients were men ($n = 49$, 61%). Regarding the histology and genetic markers, 43 subjects (54%) had a high-grade glioma, and 46 (58%) were positive for *IDH* mutation. Postcontrast enhancement was observed in 46 patients (58%), while necrosis was noted in 31 (39%). T2 FLAIR mismatch was observed in 6 patients (8%). Hemorrhage was present in 24 patients (30%). Finally, elevated relative CBF was present in 44 patients (55%). Detailed data regarding the included cohort are shown in Table 1.

Prediction of *IDH* Status

We explored the discriminative power of the diffusion metrics in relation to *IDH* status. Our findings demonstrated significant differences in the SMT characteristics between *IDH*-mutant and *IDH*-wild-type gliomas. The SMT metrics with the highest diagnostic performance in the determination of *IDH* status were microscopic fractional anisotropy (μ FA), microscopic fractional anisotropy to the third power (μ FA³), and intraneurite volume fraction (INVF), all with AUC = 0.91 (95% CI, 0.84–0.98; $P < .001$), followed by transverse microscopic diffusivity (TMD), with AUC = 0.87 (95% CI, 0.79–0.95; $P < .001$). Among the non-SMT metrics, the best-performing was mean kurtosis tensor (MKT), with AUC = 0.91 (95% CI, 0.84–0.98; $P < .001$) and mean kurtosis (MK) and radial kurtosis (RK), both with AUC = 0.90 (95% CI, 0.83–0.97; $P < .001$). For reference, ADC showed AUC = 0.82 (95% CI, 0.73–0.92; $P < .001$).

The investigated nondiffusion imaging parameter with the highest diagnostic performance was the presence of necrosis (AUC = 0.85, 95% CI, 0.77–0.94; $P < .001$). For more detailed results, please see Table 2 and Fig 3.

Prediction of Histologic Grade

Next, we examined the predictive power of the investigated diffusion metrics toward glioma grade. The best diffusion-based

predictors of grade in our study were INVF, μ FA, μ FA³ all with AUC = 0.94 (95% CI, 0.88–0.99; $P < .001$). Among the highest-scoring non-SMT metrics, MKT performed with the best with AUC = 0.94 (95% CI, 0.88–0.99; $P < .001$), along with RK and MK, both with AUC = 0.93 (95% CI, 0.88–1.00; $P < .001$) and axial kurtosis (AK) with AUC = 0.93 (95% CI, 0.87–1.00;

$P < .001$). The ADC model had AUC = 0.88 (95% CI, 0.80–0.96; $P < .001$). Detailed results regarding the prediction of histologic grade are presented in Table 3 and Fig 4.

To provide a comprehensive overview of the complex relationships among various advanced diffusion parameters, we have included a detailed correlation matrix (Online Supplemental Data).

Table 2: Comparative diagnostic accuracy of investigated parameters differentiating IDH-mutant from IDH-wild-type gliomas^a

Models and Parameters	AUC	95% CI	Optimal Cutoff	Sensitivity (%)	Specificity (%)	P Value
Nondiffusion						
Enhancement ^b	0.77	0.66–0.88	0.5 ↓	88.2	65.2	<.001
Necrosis ^b	0.85	0.77–0.94	0.5 ↓	79.4	91.3	<.001
T2LFM ^b	0.57	0.44–0.70	0.5 ↑	13.0	100	.03
Hemorrhage ^b	0.78	0.67–0.88	0.5 ↓	61.8	93.5	<.001
ADC						
ADC ^c	0.82	0.73–0.92	1.206 ↑	67.4	91.2	<.001
DTI						
FA	0.59	0.45–0.73	0.174 ↓	50.0	82.6	.050
MD ^c	0.83	0.75–0.92	0.945 ↑	89.1	64.7	<.001
DKI						
AK	0.90	0.83–0.97	0.583 ↓	88.2	84.8	<.001
RK	0.90	0.83–0.97	0.593 ↓	94.1	78.3	<.001
MK	0.90	0.83–0.97	0.567 ↓	94.1	78.3	<.001
KFA	0.55	0.42–0.68	0.807 ↑	63.2	84.2	.73
MKT	0.91	0.84–0.98	0.619 ↓	88.2	84.8	<.001
SMT						
LMD ^c	0.62	0.48–0.75	2.967 ↑	73.9	58.8	.009
TMD ^c	0.87	0.79–0.95	0.528 ↑	78.3	91.2	<.001
μ FA	0.91	0.84–0.98	0.535 ↓	91.2	84.8	<.001
μ FA ³	0.91	0.84–0.98	0.153 ↓	91.2	84.8	<.001
MMD ^c	0.85	0.77–0.94	1.369 ↑	67.4	91.2	<.001
INVF	0.91	0.84–0.98	0.339 ↓	91.2	84.8	<.001
ID ^c	0.72	0.61–0.83	2.006 ↑	69.6	70.6	<.001
ETMD ^c	0.77	0.66–0.87	1.301 ↑	76.1	67.6	<.001
EMMD ^c	0.65	0.53–0.78	1.502 ↑	67.4	67.6	.01

Note:—T2LFM indicates T2-FLAIR mismatch; FA, fractional anisotropy; MD, mean diffusivity; KFA, kurtosis fractional anisotropy; LMD, longitudinal microscopic diffusivity; μ FA³, microscopic fractional anisotropy to the third power; MMD, microscopic mean diffusivity; ID, intrinsic diffusivity, ETMD, extra-neurite transverse microscopic diffusivity; EMMD, extra-neurite microscopic mean diffusivity.

^a Optimal cutoff levels to predict IDH type were assessed by the Youden index. Cutoffs were evaluated by sensitivity and specificity. An upward arrow (↑) indicates a positive correlation, in which values above the cutoff point predict an IDH-mutant glioma, whereas a downward arrow (↓) indicates a negative correlation, in which values below the cutoff point predict an IDH-mutant glioma. P values were computed by comparing the AUC against chance performance.

^b Binary variable, indicating the presence or absence of the feature.

^c Units in mm²/s × 10⁻³.

DISCUSSION

In this study, we investigated for the first time the potential of the SMT in predicting 2 crucial factors in glioma characterization: tumor grade and IDH status. To evaluate its clinical potential, we compared the diagnostic performance of SMT with other, more established diffusion MR techniques. Our findings suggest that SMT has significant potential for characterizing adult-type gliomas. Notably, several parameters, specifically μ FA, μ FA³, and INVF demonstrated considerable predictive capabilities, each achieving a high AUC of 0.94 in predicting glioma grade and 0.91 for IDH status, indicating their potential clinical utility ($P < .001$).

In particular, our results emphasize the utility of μ FA, a metric designed to quantify the degree of directionality of water diffusion independent of axonal orientation dispersion. μ FA provides insights into the cellular and extracellular architecture of the tissue, unconfounded by the surrounding axonal microstructure.^{14,15} In the context of gliomas, IDH mutations are known to induce distinct biologic alterations, including changes in cellular density, morphology, and the organization of the extracellular matrix.^{23,24} These changes in the glioma microenvironment result in decreased directionality

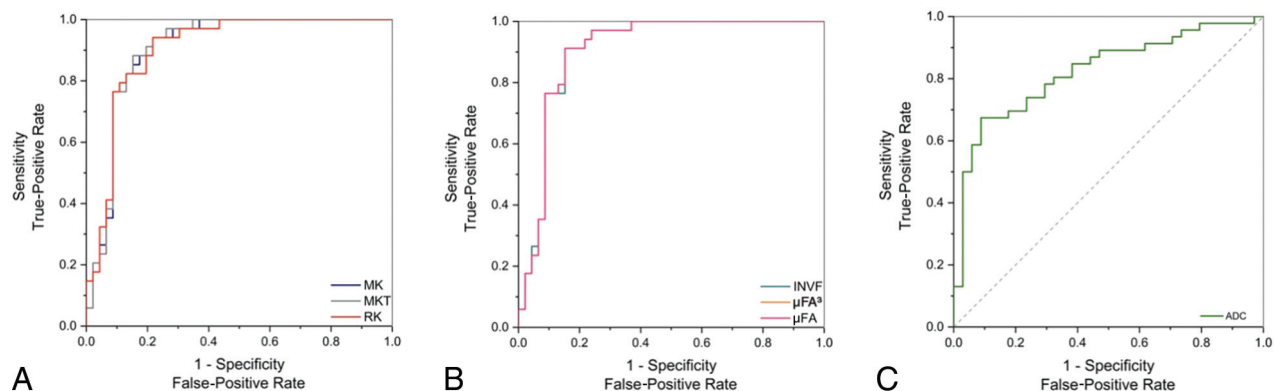


FIG 3. ROC curves for selected parameters illustrating the diagnostic accuracy in determining IDH status. The curves compare DKI (A), SMT parameters (B), and the standard clinically used ADC method (C), with an emphasis on parameters with AUC values of >0.90.

Table 3: Comparative diagnostic accuracy of investigated parameters differentiating glioma grades^a

Models and Parameters	AUC	95% CI	Optimal Cutoff	Sensitivity (%)	Specificity (%)	P Value
Nondiffusion						
Enhancement ^b	0.76	0.65–0.87	0.5 ↑	81.4	70.2	<.001
Necrosis ^b	0.81	0.71–0.91	0.5 ↑	67.4	94.6	<.001
T2LFM ^b	0.58	0.46–0.71	0.5 ↓	16.2	100	.006
Hemorrhage ^b	0.73	0.61–0.84	0.5 ↑	51.2	94.6	<.001
ADC						
ADC ^c	0.88	0.80–0.96	1.217 ↓	75.7	88.4	<.001
DTI						
FA	0.64	0.52–0.77	0.174 ↑	46.5	86.5	.01
MD ^c	0.88	0.80–0.95	1.134 ↓	83.8	76.7	<.001
DKI						
AK	0.93	0.87–1.00	0.494 ↑	97.7	75.7	<.001
RK	0.93	0.88–1.00	0.627 ↑	83.7	91.9	<.001
MK	0.93	0.88–1.00	0.539 ↑	93.0	81.1	<.001
KFA	0.53	0.40–0.67	0.219 ↓	78.4	44.2	.85
MKT	0.94	0.88–0.99	0.564 ↑	88.4	86.5	<.001
SMT						
LMD ^c	0.66	0.53–0.79	2.967 ↓	83.8	55.8	<.001
TMD ^c	0.91	0.84–0.97	2.958 ↓	91.9	79.1	<.001
μ FA	0.94	0.88–0.99	0.509 ↑	90.7	86.5	<.001
μ FA ³	0.94	0.88–0.99	0.132 ↑	90.7	86.5	<.001
MMD ^c	0.90	0.83–0.97	1.311 ↓	89.2	76.7	<.001
INVF	0.94	0.88–0.99	0.319 ↑	90.7	86.5	<.001
ID ^c	0.77	0.67–0.88	1.946 ↓	83.8	65.1	<.001
ETMD ^c	0.82	0.72–0.91	1.208 ↓	94.6	60.5	<.001
EMMD ^c	0.72	0.60–0.84	1.502 ↓	75.7	67.4	<.001

Note:—T2LFM indicates T2 FLAIR mismatch; FA, fractional anisotropy; MD, mean diffusivity; KFA, kurtosis fractional anisotropy; LMD, longitudinal microscopic diffusivity; μ FA³, microscopic fractional anisotropy to the third power; MMD, microscopic mean diffusivity; ID, intrinsic diffusivity; ETMD, extraneurite transverse microscopic diffusivity; EMMD, extraneurite microscopic mean diffusivity.

^aOptimal cutoff levels to predict glioma grade (low-grade versus high-grade) were assessed by the Youden index. Cutoffs were evaluated by sensitivity and specificity. An upward arrow (↑) indicates a positive correlation, in which values above the cutoff point predict a high-grade glioma, whereas a downward arrow (↓) indicates a negative correlation, in which values below the cutoff point predict a high-grade glioma. P values were computed by comparing the AUC against chance performance.

^bBinary variable, indicating the presence or absence of the feature.

^cUnits $\text{mm}^2/\text{s} \times 10^{-3}$.

and lower coherence of water diffusion patterns, with lower μ FA values being associated with the presence of an *IDH* mutation. Our findings demonstrate that μ FA is particularly adept at detecting these variations, reinforcing its potential as a diagnostic tool in assessing glioma characteristics.

Another notable finding is the robust relationship between INVf and *IDH* status. INVf is designed to quantify the fraction of the voxel occupied by intraneurite space, essentially reflecting the density of neurite-like structures within the tumor microenvironment. However, the underlying reasons for its significant association with *IDH* status remain unclear. A possible explanation could be that tissue changes, more commonly observed in aggressive glioma variants, are perceived to have axon-like diffusion properties by the SMT model, causing the strong correlation. Alternatively, the association may be a result of modeling constraints imposed on the INVf parameter by the SMT model. Microstructural models, including SMT, typically assume that bodily tissues can be described as finite, often a small sum of Gaussian compartments.²⁵ This approach, while necessary for practical reasons (eg, computational time), oversimplifies the complex nature of brain tissue and its intra- and extracellular compartments. Consequently,

this simplification may result in the decreased specificity of parameters attempting to characterize portions of these compartments.

The study also revealed a strong predictive performance of SMT metrics in the evaluation of glioma grade. These results further confirm that diffusion parameters may reflect the underlying pathologic processes of gliomas, such as cellularity,¹⁰ which are critical determinants of tumor grade.

Our findings regarding the utility of ADC and DKI in glioma characterization align with previous studies,^{11,26} confirming the added utility of advanced diffusion imaging in the characterization of brain gliomas.

Despite these promising findings, our study has limitations. The sample size, though adequate for initial exploration, warrants expansion in future studies to enhance the generalizability of the results and provide clearer separation between the diagnostic performances of the investigated predictive features. Another potential limitation is the relatively long acquisition duration of the used diffusion sequence. While still within the limits of clinical feasibility, an addition of a 9-minute pulse sequence may not be feasible for many centers. However, our study design intentionally included a robust diffusion sequence, and SMT parameters

can be reconstructed using only 2 nonzero b-values, instead of 6 used in our study. The reduction of number of b-values in combination with SNR²⁷ and angular resolution²⁸ enhancing algorithms can significantly reduce scanning times to more manageable clinical durations of about 2–3 minutes.

Integrating SMT with other emerging imaging modalities, such as amino acid PET, chemical exchange saturation transfer (CEST) MRI, and MR spectroscopy, could further refine the non-invasive characterization of gliomas. The inclusion of CEST MRI, which offers surrogate biomarkers for amides and amines crucial in glioma subtyping, could provide a valuable enhancement to our imaging arsenal, as evidenced by the work of Mancini et al.²⁹ Similarly, the application of machine-learning algorithms,^{30,31} other advanced diffusion techniques (eg, neurite orientation dispersion and density imaging [NODDI]),³² or higher-field-strength MR spectroscopy could provide a more detailed metabolic profile of gliomas, enhancing our understanding of their unique characteristics and aiding in more accurate grading.

Investigating the longitudinal changes in SMT parameters during treatment and follow-up could provide valuable information on tumor response and progression. This would be particularly useful in assessing the efficacy of targeted therapies

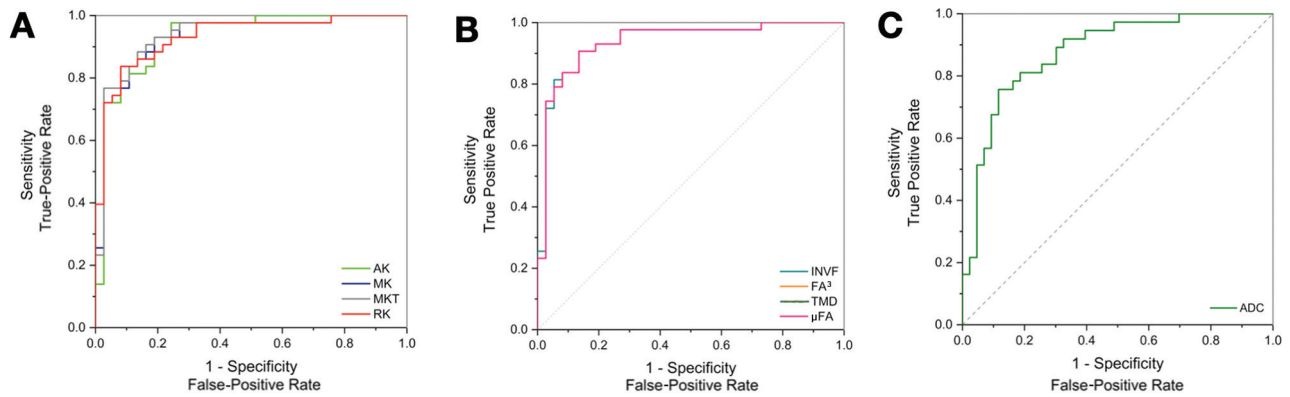


FIG 4. ROC curves for selected parameters illustrating the diagnostic accuracy in determining glioma grade. The curves compare DKI (A), and SMT (B), parameters with the standard clinically used ADC method (C), with an emphasis on parameters with AUC values of 0.90.

that might influence tumor microstructure in a manner different from traditional chemoradiation.

Finally, the development of automated, artificial intelligence-driven algorithms for SMT parameter analysis could facilitate the translation of this technique into routine research or even clinical practice, making it more accessible for widespread use.

CONCLUSIONS

Our study underscores the potential of SMT as a significant non-invasive tool for predicting *IDH* status and tumor grading in adult-type diffuse gliomas, enhancing preoperative tumor characterization and potentially influencing treatment decisions and outcomes. The diagnostic performance of SMT parameters, despite certain limitations, offers promising avenues for advancing glioma diagnostics. Future directions should focus on refining microstructural models to better understand the biologic underpinnings of SMT measurements, expanding sample sizes, and incorporating advanced imaging modalities to enrich the non-invasive assessment of gliomas. Additionally, investigating the changes in the model parameters during treatment could offer insights into tumor response and progression, thereby contributing to more tailored and effective therapeutic strategies.

Disclosure forms provided by the authors are available with the full text and PDF of this article at www.ajnr.org.

REFERENCES

- Di Carlo DT, Duffau H, Cagnazzo F, et al. **IDH wild-type WHO grade II diffuse low-grade gliomas; a heterogeneous family with different outcomes: systematic review and meta-analysis.** *Neurosurg Rev* 2020;43:383–95 [CrossRef Medline](#)
- Louis DN, Perry A, Reifenberger G, et al. **The 2016 World Health Organization Classification of Tumors of the Central Nervous System: a summary.** *Acta Neuropathol* 2016;131:803–20 [CrossRef Medline](#)
- Uetani H, Azuma M, Khant ZA, et al. **Importance of age and non-contrast-enhancing tumor as biomarkers for isocitrate dehydrogenase-mutant glioblastoma: a multicenter study.** *J Comput Assist Tomogr* 2023;47:659–65 [CrossRef Medline](#)
- Jensen JH, Helpert JA, Ramani A, et al. **Diffusional kurtosis imaging: the quantification of non-gaussian water diffusion by means of magnetic resonance imaging.** *Magn Reson Med* 2005;53:1432–40 [CrossRef Medline](#)
- Le Bihan D. **Molecular diffusion nuclear magnetic resonance imaging.** *Magn Reson Q* 1991;7:1–30 [Medline](#)
- Darbar A, Waqas M, Enam SF, et al. **Use of preoperative apparent diffusion coefficients to predict brain tumor grade.** *Cureus* 2018;10:e2284 [CrossRef Medline](#)
- Zulfiqar M, Yousem DM, Lai H. **ADC values and prognosis of malignant astrocytomas: does lower ADC predict a worse prognosis independent of grade of tumor? A meta-analysis.** *AJR Am J Roentgenol* 2013;200:624–29 [CrossRef Medline](#)
- Eidel O, Neumann JO, Burth S, et al. **Automatic analysis of cellularity in glioblastoma and correlation with ADC using trajectory analysis and automatic nuclei counting.** *PLoS One* 2016;11:e0160250 [CrossRef Medline](#)
- Gauvain KM, McKinstry RC, Mukherjee P, et al. **Evaluating pediatric brain tumor cellularity with diffusion-tensor imaging.** *AJR Am J Roentgenol* 2001;177:449–54 [CrossRef Medline](#)
- Abdalla G, Dixon L, Sanverdi E, et al. **The diagnostic role of diffusional kurtosis imaging in glioma grading and differentiation of gliomas from other intra-axial brain tumours: a systematic review with critical appraisal and meta-analysis.** *Neuroradiology* 2020; 62:791–802 [CrossRef Medline](#)
- Szczepankiewicz F, Lasič S, van Westen D, et al. **Quantification of microscopic diffusion anisotropy disentangles effects of orientation dispersion from microstructure: applications in healthy volunteers and in brain tumors.** *Neuroimage* 2015;104:241–52 [CrossRef Medline](#)
- Smith SM, Nichols TE, Vidaurre D, et al. **A positive-negative mode of population covariation links brain connectivity, demographics and behavior.** *Nat Neurosci* 2015;18:1565–67 [CrossRef Medline](#)
- Hagmann P, Grant PE, Fair DA. **MR connectomics: a conceptual framework for studying the developing brain.** *Front Syst Neurosci* 2012;6:43 [CrossRef Medline](#)
- Kaden E, Kelm ND, Carson RP, et al. **Multi-compartment microscopic diffusion imaging.** *Neuroimage* 2016;139:346–59 [CrossRef Medline](#)
- Kaden E, Kruggel F, Alexander DC. **Quantitative mapping of the per-axon diffusion coefficients in brain white matter.** *Magn Reson Med* 2016;75:1752–63 [CrossRef Medline](#)
- By S, Xu J, Box BA, et al. **Multi-compartmental diffusion characterization of the human cervical spinal cord in vivo using the spherical mean technique.** *NMR Biomed* 2018;31:e3894 [CrossRef Medline](#)
- Tournier JD, Smith R, Raffelt D, et al. **MRtrix3: a fast, flexible and open software framework for medical image processing and visualisation.** *Neuroimage* 2019;202:116137 [CrossRef Medline](#)
- Veraart J, Novikov DS, Christiaens D, et al. **Denoising of diffusion MRI using random matrix theory.** *Neuroimage* 2016;142:394–406 [CrossRef Medline](#)
- Kellner E, Dhital B, Kiselev VG, et al. **Gibbs-ringing artifact removal based on local subvoxel-shifts.** *Magn Reson Med* 2016;76:1574–81 [CrossRef Medline](#)

20. Andersson JL, Sotiropoulos SN. **An integrated approach to correction for off-resonance effects and subject movement in diffusion MR imaging.** *Neuroimage* 2016;125:1063–78 [CrossRef Medline](#)
21. Andersson JL, Skare S, Ashburner J. **How to correct susceptibility distortions in spin-echo echo-planar images: application to diffusion tensor imaging.** *Neuroimage* 2003;20:870–88 [CrossRef Medline](#)
22. Tustison NJ, Avants BB, Cook PA, et al. **N4ITK: improved N3 bias correction.** *IEEE Trans Med Imaging* 2010;29:1310–20 [CrossRef Medline](#)
23. Wang X, Zhou C, Wang L, et al. **Motor cortex gliomas induces microstructural changes of large fiber tracts revealed by TBSS.** *Sci Rep* 2020;10:16900–08 [CrossRef Medline](#)
24. Marino S, Menna G, Di Bonaventura R, et al. **The extracellular matrix in glioblastomas: a glance at its structural modifications in shaping the tumoral microenvironment: a systematic review.** *Cancers (Basel)* 2023;15:1879 [CrossRef Medline](#)
25. Henriques RN, Jespersen SN, Shemesh N. **Microscopic anisotropy misestimation in spherical-mean single diffusion encoding MRI.** *Magn Reson Med* 2019;81:3245–61 [CrossRef Medline](#)
26. Wang QP, Lei DQ, Yuan Y, et al. **Accuracy of ADC derived from DWI for differentiating high-grade from low-grade gliomas: systematic review and meta-analysis.** *Medicine (Baltimore)* 2020;99:e19254 [CrossRef Medline](#)
27. Fadnavis S, Batson J, Garyfallidis E. **2020 Patch2Self: Denoising Diffusion MRI with Self-Supervised Learning.** In: Larochelle H, Ranzato M, Hadsell R, Balcan MF, Lin H, eds, *Advances in Neural Information Processing Systems*; vol. 33: 16293–303. Curran Associates, Inc
28. Michailovich O, Rathi Y, Dolui S. **Spatially regularized compressed sensing for high angular resolution diffusion imaging.** *IEEE Trans Med Imaging* 2011;30:1100–15 [CrossRef Medline](#)
29. Mancini L, Casagrande S, Gautier G, et al. **CEST MRI provides amide/amine surrogate biomarkers for treatment-naïve glioma sub-typing.** *Eur J Nucl Med Mol Imaging* 2022;49:2377–91 [CrossRef Medline](#)
30. Eichinger P, Alberts E, Delbridge C, et al. **Diffusion tensor image features predict IDH genotype in newly diagnosed WHO grade II/III gliomas.** *Sci Rep* 2017;7:13396 [CrossRef Medline](#)
31. Sakai Y, Yang C, Kihira S, et al. **MRI radiomic features to predict IDH1 mutation status in gliomas: a machine learning approach using gradient tree boosting.** *Int J Mol Sci* 2020;21:8004 [CrossRef Medline](#)
32. Zhang H, Schneider T, Wheeler-Kingshott CA, et al. **NODDI: practical in vivo neurite orientation dispersion and density imaging of the human brain.** *Neuroimage* 2012;61:1000–16 [CrossRef Medline](#)